MetaResource

DOI 10.23919/METAR.2026.000041

Review Article

High-temperature magnetic sensors for mineral exploration

Zhaozhong Zhang, Zilong Zhang, Guo Chen, and Meiyong Liao(✉)

***MetaResource*, Just Accepted Manuscript** • 10.23919/METAR.2026.000041

https://publish.cnki.net/chain on April 10, 2026

Just Accepted

High-temperature magnetic sensors for mineral exploration

Zhaozhong Zhang, Zilong Zhang, Guo Chen, Meiyong Liao*
Research Center for Electronic and Optical Materials, National Institute for Materials Science, Namiki 1-1, Tsukuba, Ibaraki 3050044, Japan
Address correspondence to Meiyong.Liao@nims.go.jp

ABSTRACT

Magnetic sensing is a non-invasive and cost-effective technique widely used in geophysical mineral exploration, exploiting spatial variations in the Earth's magnetic field to identify subsurface magnetic contrasts. As exploration targets shift toward deeper ore bodies and geothermal environments, the demand for reliable high-temperature magnetic sensors continues to grow. This review examines high-temperature magnetic sensing technologies for mineral exploration, focusing on four major categories of solid-state and miniaturized sensors: fluxgate, Hall effect, magnetoresistive (MR), and microelectromechanical systems (MEMS) sensors. The underlying detection mechanisms, material developments, device architectures, and sensing performance of each technology are discussed. Particular attention is given to material innovations enabling stable operation in harsh environments, including wide-bandgap semiconductors for Hall sensors, advanced magnetic alloys for MR devices, and diamond-based magnetostrictive MEMS structures. Applications across ground, airborne, marine, and borehole platforms are reviewed. Finally, current challenges and future trends are outlined, discussing the increasing role of data-driven approaches for intelligent mineral exploration.

Key words: Mineral exploration, magnetic sensors, high temperatures, wide bandgap semiconductors, MEMS

1. Introduction

Magnetic minerals on Earth are present in various types of rocks, meteorites, sediments, and soils[1]. Their magnetic properties mainly originate from magnetic susceptibility and remanent magnetization, which, within the Earth's crust, are predominantly controlled by the distribution of iron-bearing magnetic minerals[2]. The magnetic method, one of the oldest techniques in geophysical exploration, has been effectively employed for mineral detection and exploration, offering advantages such as high efficiency, low cost, and non-invasiveness. The fundamental principle of magnetic sensing in mineral exploration is to measure subtle spatial variations in the Earth's magnetic field to infer subsurface magnetic contrasts [3]. Early magnetic surveys using mechanical methods like magnetic force balance were primarily qualitative, aimed at locating magnetite-rich iron ores and basic intrusions[4]. The development of fluxgate and proton precession magnetometers enabled high-precision measurements and systematic regional surveys, marking the transition to quantitative and large-scale magnetic exploration [3]. Over the past decades, next-generation magnetic sensors have significantly extended the capabilities of magnetic exploration. Quantum-based sensors, including optically pumped magnetometers (OPMs) and superconducting quantum interference devices (SQUIDs), achieve sub-nanotesla ($1nT=10^{-9}T$) to femtotesla-level ($1fT=10^{-15}T$) sensitivity, allowing detection of deep and weakly magnetized ore bodies. Optically pumped magnetometers operate at room temperature, offering high sensitivity and fast temporal response, making them particularly suitable for low-altitude airborne applications [5]. SQUIDs represent the ultimate sensitivity limit and remain indispensable for extremely weak magnetic field detection [6]. Meanwhile, solid-state magnetoresistive sensors exhibit advantages in miniaturization, low-power consumption, and array integration, enabling Unmanned Aerial Vehicle (UAV)-borne, downhole, and multi-channel magnetic systems. The rapid development of quantum and miniaturized solid-state sensors, coupled with autonomous and intelligent platforms, has been reshaping the technical capabilities and operational paradigms of magnetic exploration.

Importantly, reliable high-temperature magnetic sensors are increasingly in demand not only to withstand extreme geothermal gradients in deep mineral exploration but also to enable advanced airborne and UAV platforms. In compact airborne platforms, high-temperature magnetic sensors provide superior thermal stability without the need for bulky cooling systems, enabling extreme miniaturization and flexible integration within space-constrained airborne instruments. This imposes additional requirements on sensor materials, thermal compensation, and multi-sensor integration, particularly for downhole and borehole applications targeting deeply buried or geothermal-affected ore systems.

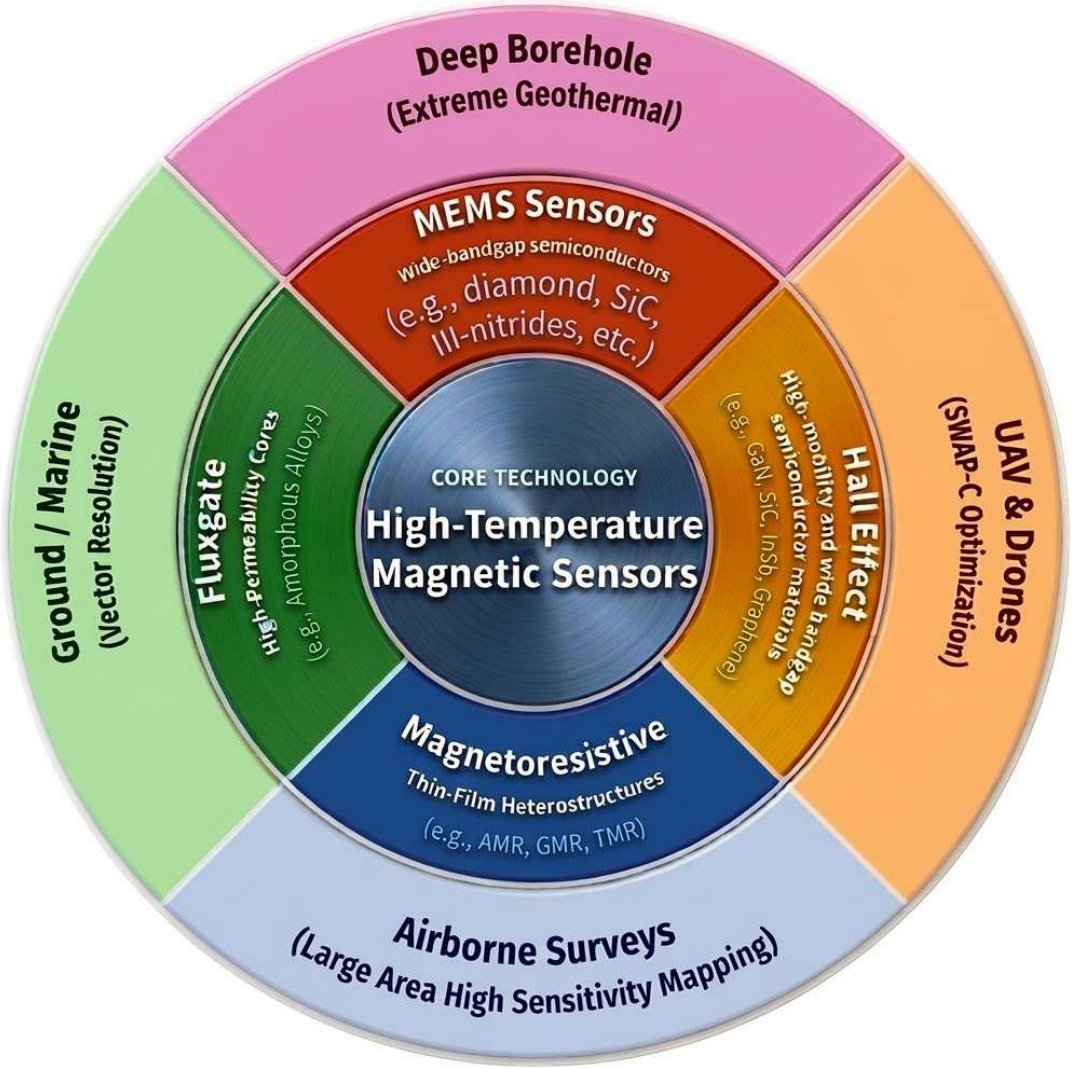

Figure 1 High-temperature magnetic sensors for advanced mineral exploration. The inner ring categorizes the four primary solid-state sensing technologies, MEMS, Hall effect, magnetoresistive, and fluxgate. The outer ring connects these fundamental device architectures to their strategic exploration platforms, ranging from deep borehole logging in extreme geothermal environments to SWaP-C (Size, Weight, Power, and Cost) optimized autonomous UAVs and regional airborne surveys.

This review aims to provide an overview of high-temperature magnetic sensing technologies in mineral exploration (Figure 1). While SQUIDs hold immense value in mineral exploration due to their unparalleled magnetic field sensitivity, these quantum sensors require cryogenic cooling, typically immersion in liquid helium or liquid nitrogen. Interested readers are directed to reported literature [6]. Here, we mainly focus on fluxgate sensors, Hall sensors, magnetoresistive sensors, and microelectromechanical systems

(MEMS) sensors. The physical detection mechanisms, materials, devices, sensing performance, and the applications of these sensors in mineral exploration will be introduced. We also discuss challenges and future trends of magnetic sensors in mineral exploration.

2. Principles of high-temperature magnetic sensors

2.1 Fluxgate sensors

Fluxgate magnetometers represent one of the most mature and widely deployed technologies in geophysical magnetic surveying. Typical fluxgate sensors operate over a magnetic field range from approximately 100 pT to 100 mT [7]. Commercially available fluxgate magnetometers typically exhibit resolution of 100 pT ~ nT. They can detect subtle variations in the Earth's magnetic field caused by ferromagnetic minerals, magnetite-rich formations, and ore-controlling geological structures. By measuring either total magnetic intensity or individual vector components, fluxgate magnetometers provide critical information for identifying magnetically anomalous regions associated with mineral deposits.

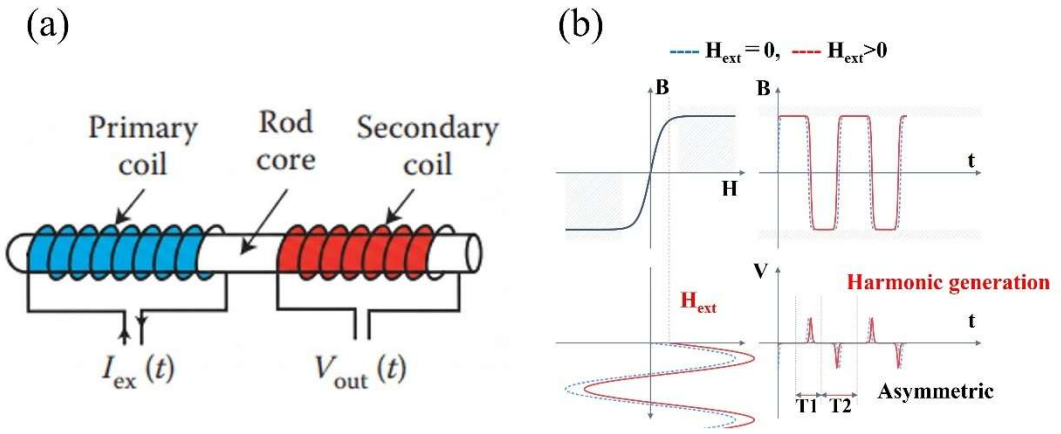

Figure 2 Principle of the fluxgate sensor. (a) the single-rod structure contains a primary driving coil for excitation and a secondary coil for sensing. (b) Under the external magnetic field H_{ext}, core magnetization is biased, which induces a second harmonic voltage in the sensing coil.

A fluxgate sensor operates based on the nonlinear magnetization characteristics of a soft ferromagnetic core combined with Faraday's law of electromagnetic induction. As illustrated in Figure 2, a typical configuration consists of a soft magnetic core surrounded by an excitation (drive) coil and a sensing (pickup) coil. An alternating current applied to the drive coil periodically drives the core into positive and negative magnetic saturation.

In the absence of an external magnetic field, the magnetization cycle of the core is symmetric, resulting in no second-harmonic component in the sensing coil output. When an external magnetic field is present, it biases the core magnetization, resulting in an asymmetry in the magnetic response. This asymmetry induces a second harmonic voltage in the sensing coil, which is proportional to the external field strength. Fluxgate sensors can thus provide highly linear, vector-resolved measurements of magnetic fields with low noise levels. The voltage output of a fluxgate sensor with a constant coil area A is expressed as [7, 8]

$$V_{sens} = A\mu_0\mu_r N_s \frac{dH(t)}{dt} + A\mu_0 H N_s \frac{d\mu_r(t)}{dt} \quad (1)$$

where V_{sens} is the induced voltage of the sensing coil, H is the applied magnetic field, Ns is the number of turns of the coil, μ_0 is the permeability of vacuum, and μ_r is the relative permeability of the magnetic coil.

The performance of fluxgate sensors, specifically their sensitivity and noise floor, is primarily dictated by the magnetic properties of the core material and the precision of the coil geometry. Fluxgate magnetometers can be rod-core, ring-core, racetrack, and planar microfabricated configurations [7, 9]. The core is typically made of high-permeability and low coercivity soft magnetic materials, such as permalloy (NiFe alloys) or cobalt-based amorphous metals (e.g. CoFeSiB ribbons), which offer high saturation induction and minimal hysteresis as well as low magnetostriction, low intrinsic noise and eddy currents[10]. Recent advances have incorporated nanocrystalline cores with superior magnetic permeability and reduced noise. The drive and sensing coils are typically copper, with careful winding to minimize parasitic inductances and thermal effects. Modern fluxgate sensors may also integrate miniaturized electronics for signal amplification, temperature compensation, and digital conversion, enabling compact and lightweight devices suitable for airborne or UAV-mounted surveys.

Fluxgate sensors are characterized by high sensitivity, low noise, and bandwidth from DC to several kilohertz [11]. Device structures have evolved from bulky conventional rods to integrated microtechnology and PCB designs. At room temperature, the noise level can be as low as 6pT/√Hz for a racetrack shaped fluxgate sensors with a core of $(CoFe)_{70}(MoSiB)_{30}$ amorphous metal [12]. Miniaturized triaxial configurations (e.g. 23x23x21 cm^3) by using Co-Fe-Si-B amorphous wire allow for high-temperature operation up to 175ºC with noise level of 200 pT/√Hz . The operation temperature up to 250ºC was also demonstrated with a temperature coefficient of 6.8×10^{-4} /ºC, making them suitable for high-temperature magnetic sensing[13, 14]. Such characteristics make fluxgate sensors suitable for harsh geological environments, including deep borehole

surveys. In mineral exploration, fluxgate systems are particularly effective for detecting moderate to large-scale magnetic anomalies associated with magnetite-rich ore bodies, magmatic sulfide deposits, and hydrothermal alteration zones. Ground-based fluxgate surveys provide high-resolution mapping of near-surface structures, while airborne fluxgate systems mounted on fixed-wing aircraft or helicopters allow rapid regional reconnaissance over inaccessible or rugged terrain[15].

Despite their advantages, fluxgate sensors have several limitations. Their physical size and weight, especially in high-sensitivity vector configurations, can restrict deployment of small UAVs[16]. They require low-noise electronics and careful thermal management to maintain stability, particularly in fluctuating environmental conditions. The drive current generates minor magnetic fields, which need to be compensated for or accounted for in high-precision surveys. Although the increasing excitation frequency can improve sensitivity, the eddy current becomes the issue.

Fluxgate magnetometers remain a cornerstone of magnetic exploration, offering reliable, vector-resolved measurements with moderately high sensitivity and low noise. Their robustness, established design, and adaptability to both ground-based and airborne surveys make them promising for mapping large-scale lithological variations, ore-controlling structures, and magnetically significant anomalies. Continuous improvements in core materials, miniaturization, and electronics integration are extending their capabilities, ensuring that fluxgate sensors continue to play a central role in the exploration of both near-surface and deeper mineral deposits.

2.2. Hall effect sensors

Hall effect sensors are a foundational technology in solid-state magnetometry, widely utilized for measuring magnetic fields in industrial, automotive, biomedical, and geophysical applications. Their utility in mineral exploration stems from their solid-state robustness, compactness, and ability to provide absolute measurements of the Earth's magnetic field. Depending on device design, Hall sensors can measure magnetic fields ranging from several microtesla to Tesla.

The Hall sensors operate based on the classical Hall effect, discovered by Edwin Hall in 1879 [17]. As shown in Figure 3, a Hall device consists of a thin conductive or semiconductive layer through which a current I_x flows along one axis. When a perpendicular magnetic field B_z is applied, the Lorentz force deflects charge carriers, leading to charge accumulation and the generation of a transverse electric field. This produces a measurable Hall voltage V_H across the orthogonal axis.

$$V_H = \frac{I_x B_z}{qnt} \quad (2)$$

where q is the charge, n is the carrier density, and t is the thickness of the conductor or semiconductor.

The Hall coefficient is defined as:

$$R_H = \frac{E_y}{j_x B_z} \quad (3)$$

where j_x is the current density and E_y is the induced electric field.

For semiconductors in which both electrons and holes contribute to conduction, the Hall coefficient becomes

$$R_H = \frac{n_h \mu_h^2 - n_e \mu_e^2}{e(n_h \mu_h + n_e \mu_e)^2} \quad (4)$$

where n_h and n_e are the hole and electron densities, μ_h and μ_e are their respective mobilities.

The originally observed Hall phenomenon is referred to as the Ordinary Hall Effect (OHE). Additional Hall effects, including Anomalous Hall Effect (AHE), Quantum Hall Effect (QHE), Quantum Spin Hall Effect (QSHE), and Quantum Anomalous Hall Effect (QAHE), have been reported, though ordinary Hall effect has been used in mineral exploration [18].

In metals, the Hall coefficient is typically small due to high carrier density, resulting in low sensitivity. Therefore, most Hall sensors are based on semiconductors. Traditional Hall devices are predominantly fabricated from silicon due to its mature CMOS-compatible processing and low cost. To enhance sensitivity, narrow bandgap semiconductors such as InSb, InAs, and InGaAs have been employed because of their higher carrier mobilities [19-23]. To enable operation in harsh environments, wide-bandgap semiconductors such as gallium nitride (GaN), silicon carbide (SiC), and diamond have been adopted [24-27]. GaN-based Hall sensors exploit high electron mobility and wide bandgap properties to maintain sensitivity and low noise at elevated temperatures (typically 300–400°C) [26, 28-32], making them suitable for geothermal or deep-drilling applications. SiC Hall devices and circuits have demonstrated reliable operation from room temperature up to 500°C [33, 34], with short-term functionality reported up to 600°C. Noise densities on the order of ~1 μT/√Hz at 500°C have been reported [35], highlighting their suitability for high-temperature magnetic sensing in harsh geological environments.

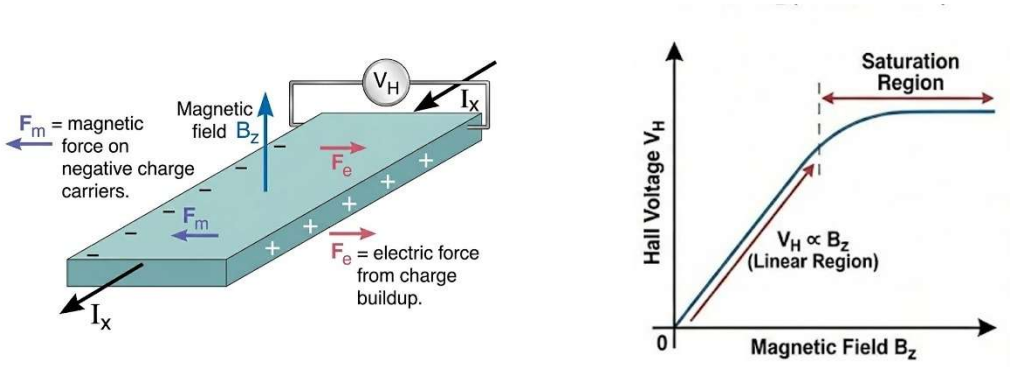

Figure 3 The principle of Hall sensors.

Recent research has expanded Hall sensor materials into two-dimensional (2D) materials to develop microscale and nanoscale devices. The 2D materials enable the operation of the device in low currents (nA level) with low power consumption. Graphene, with its extremely high carrier mobility and atomic thickness, enables ultra-sensitive Hall detection at room temperature, potentially reaching nanotesla-level noise at 100 kHz [36, 37]. Other 2D materials, including transition-metal dichalcogenides such as MoS_2 and WS_2, are being investigated for low-noise and potentially high-temperature applications, offering pathways toward flexible and miniaturized sensor arrays[38].

Standard planar Hall devices use a cross or Hall-bar geometry, where current flows along one axis and voltage is measured orthogonally. Vertical Hall structures have been developed to improve three-dimensional magnetic field detection[39, 40]. Integrated Hall arrays enable spatial mapping of magnetic anomalies[41]. Modern Hall sensors commonly integrate on-chip amplification, temperature compensation, and analog-to-digital conversion circuits. CMOS integration improves signal-to-noise ratio, dynamic range, and thermal stability while reducing system size[42, 43]. These developments have enabled compact, lightweight, and fully integrated sensing modules suitable for UAV platforms, portable systems, and downhole probes.

Hall sensors offer several advantages for mineral exploration. Their solid-state construction ensures mechanical robustness and resistance to vibration and the small size and light weight are beneficial for portable surveys[44]. They provide direct and linear magnetic field measurements without requiring complex excitation mechanisms. Wide-bandgap semiconductor devices enable operation at high temperatures and in chemically aggressive environments. Furthermore, planar fabrication and CMOS compatibility facilitate array configurations for spatial magnetic mapping. However, the sensitivities of Hall sensors are typically in the microtesla range, which may be insufficient for detecting ultra-weak or deeply buried magnetic anomalies. The temperature dependent mobility

requires compensation circuitry to maintain accuracy. Although emerging 2D-material Hall devices show improvements in sensitivity, large-scale fabrication, long-term stability, and field reliability remain challenges.

Overall, Hall effect sensors represent a mature yet continuously evolving class of magnetic sensing technology. From silicon-based devices to wide bandgap semiconductors for high-temperature, and further toward emerging 2D-material platforms, Hall sensors combine compactness, robustness, and moderate sensitivity. Although their performance in ultra-weak anomaly detection remains limited compared to high-sensitivity magnetometers, ongoing advances in materials, device architecture, and signal processing continue to expand their applicability in both near-surface and harsh-environment mineral exploration.

2.3 Magnetoresistive sensors

The magnetoresistance (MR) effect was first discovered in 1856 by William Thomson in ferromagnetic metals such as iron and nickel, which later became known as the anisotropic magnetoresistance (AMR) effect [45]. Magnetoresistive sensors have been widely utilized across industrial, automotive, and consumer electronics for their high sensitivity and compactness. Unlike conventional Hall sensors, which rely on the classical Hall effect, MR sensors exploit changes in electrical resistance arising from the relative orientation of magnetization and electron transport within ferromagnetic materials. This property enables enhanced sensitivity to weak or spatially subtle magnetic anomalies. As mineral exploration increasingly relies on UAV-based surveys, downhole tools, and distributed sensing arrays, compact and highly sensitive MR sensors have gained significant practical importance.

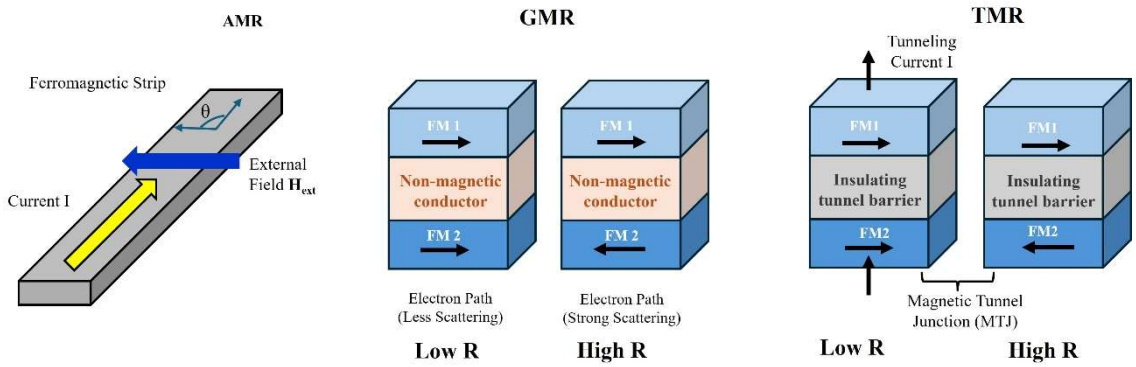

Figure 4 Operating principles of magnetoresistive sensors. AMR: Resistance changes based on the angle between current flow and magnetization direction in a ferromagnetic strip. GMR: Resistance depends on the relative magnetic orientation of ferromagnetic layers separated by a conductive spacer, caused by spin-dependent electron scattering

(Parallel=Low R, Antiparallel=High R). TMR: Resistance depends on electron tunneling through a thin insulating barrier between ferromagnetic layers, governed by their relative magnetic orientation (Parallel=High Tunneling/Low R, Antiparallel=Low Tunneling/High R).

Magnetoresistive sensors operate on the principle that the electrical resistance of a material changes in response to an applied magnetic field [46]. Depending on the device architecture and transport mechanism, MR sensors are classified into three major categories, including AMR, giant magnetoresistance (GMR), and tunneling magnetoresistance (TMR). While all three types exhibit the common principle of resistance modulation in response to an external magnetic field, they differ in their underlying physical mechanisms, materials, device architectures, and sensitivity. In Figure 4, the operation mechanisms of the MR sensors are illustrated.

The AMR effect represents the most fundamental MR effect, originating from spin-orbit coupling in bulk ferromagnetic materials, which operate based on the dependence of electrical resistivity of ferromagnetic materials on the angle between the magnetization vector and the direction of current flow [47]. When a magnetic field is applied, the magnetic domains in the ferromagnetic thin film rotate, changing the scattering of conduction electrons. This produces a change in electrical resistance that is proportional to the magnetic field magnitude. The AMR effect is expressed by the following expression:

$$\rho(\theta) = \rho_{//} + (\rho_{\perp} - \rho_{//})\rho cos^2(\theta) \quad (5)$$

where θ is the angle between the magnetic field and the electric current direction, $\rho_{\perp}$ is the perpendicular resistivity, $\rho_{//}$ is the longitudinal resistivity[48]. The ratio of $(\rho_{\perp} - \rho_{//})/\rho_{//}$ is the magnetoresistive coefficient, a key parameter to evaluate the MR sensor.

Anisotropic magnetoresistance sensors typically exhibit magnetoresistance ratios of several percent, usually below 5% at room temperature [49, 50]. The effect occurs in 3d transition metals such as Fe, Ni, and Co, as well as in alloys including NiPd, NiZn, NiZr, permalloy ($Ni_{80}Fe_{20}$), and $(Ni_{100-x}Co_x)_{86}Fe_{14}$[47, 51-53]. Among these, permalloy is most widely used due to its high permeability, low coercivity, and stable magnetoresistive response. Devices are commonly fabricated as thin ferromagnetic films deposited on silicon or glass substrates using sputtering or evaporation techniques and are arranged in Wheatstone bridge configurations to enhance sensitivity and compensate for thermal drift. “Barber pole” bias structures are often integrated to improve linearity [54]. The noise level of AMR sensors can reach approximately ~220 pT/√Hz at 1 Hz at room temperature[55]. High-temperature operation up to 225°C has been reported, although the

noise increases to approximately 2.6 nT/√Hz at 1 Hz at that temperature [56].

Anisotropic magnetoresistance sensors are characterized by structural simplicity, compact size, low cost, and relatively good high-temperature stability [57]. They are more sensitive than conventional Hall sensors and are well suited for integrated and portable systems. However, their performance is limited by a relatively low magnetoresistance ratio, a narrow intrinsic linear dynamic range, and susceptibility to thermal drift, which requires electronic compensation. Magnetic flux concentrator can be used to improve the weak-field detection capability [58].

The GMR effect is a quantum effect that was discovered independently in 1988 by two research groups, one led by Peter Grünberg in a trilayer structure of Fe/Cr/Fe [59] and the other by Albert Fert in a multilayers structure of $(Fe/Cr)_n$ on GaAs substrate, where n could be as high as 60 [60]. GMR sensors exploit the spin-dependent scattering of electrons in multilayer structures composed of alternating ferromagnetic and non-magnetic conductive layers. When the magnetizations of the ferromagnetic layers are parallel, conduction electrons with aligned spins pass through with minimal scattering, producing low resistance. When the layers are antiparallel, scattering increases, resulting in higher resistance. The GMR ratio is defined as [61]

$$MR = \frac{R_p - R_{ap}}{R_{ap}} = \frac{(R^{\uparrow} - R^{\downarrow})^2}{4R^{\uparrow}R^{\downarrow}} \quad (6)$$

where R_p and R_{ap} are the resistances of the layered system with parallel and antiparallel magnetizations, respectively, $R\uparrow$ and $R\downarrow$ are the resistances of the majority and minority electrons in a magnetic layer.

Giant magnetoresistance materials are typically realized as engineered magnetic heterostructures, most commonly in the form of multilayers or spin-valves composed of two ferromagnetic (FM) layers separated by a thin nonmagnetic (NM) metallic spacer[62]. GMR structures can achieve magnetoresistance ratios ranging from several tens to over one hundred percent, significantly exceeding those of AMR devices. Practical GMR stacks employ ferromagnetic layers such as Co, CoFe, NiFe (permalloy), or CoFeB, separated by nonmagnetic metallic spacers such as Cu, Cr, Ag, or Au. Spin-valve devices incorporate antiferromagnetic pinning layers, including IrMn, PtMn, FeMn, or NiO, to stabilize one ferromagnetic layer via exchange bias[63-66]. Granular GMR systems, such as Co–Ag, Co–Cu, or Fe–Ag composites were also reported [67, 68]. A circular GMR sensor using a Co-Ag nanogranular thin film patterned as a Wheatstone bridge on alumina exhibited ~8% MR at room temperature, which was able to operate up to 120 °C with the magnetic film itself tolerating temperatures up to ~200 °C [69]. A study on NiMn antiferromagnetic spin-valve films shows that NiMn has a blocking temperature of

~400 °C, markedly higher than typical IrMn (225ºC) pinning layers[70]. This suggests superior thermal stability and extended functional operation at elevated temperatures. GMR sensors were also fabricated on both rigid and flexible substrates and printable flakes [71, 72]. The minimum magnetic noise of GMR sensors can reach ~sub-nT/√Hz at room temperature [73].

Tunnel magnetoresistance represents the current state-of-the-art in high-sensitivity MR magnetometry. Similar in multilayer structure to GMR, TMR replaces the conductive spacer with an ultra-thin insulating layer (IL) as a barrier, forming a FM/IL/FM structured magnetic tunnel junction (MTJ)[74]. In contrast to GMR, where electron transport occurs through a metallic spacer, TMR relies on quantum tunneling through the insulating barrier. The tunneling probability, and hence the resistance, depends strongly on the relative magnetic orientation of the ferromagnetic layers. When the magnetizations are parallel, tunneling probability is high and resistance is low; when antiparallel, tunneling probability decreases and resistance increases. TMR ratio is defined as the relative change in electrical resistance of a MTJ when the magnetic alignment of its two ferromagnetic electrodes switches between parallel (P) and antiparallel (AP) configurations [71].

$$TMR = \frac{R_{AP} - R_P}{R_P} = \frac{2P_1P_2}{1-P_1P_2} \quad (7)$$

where R_P and R_{AP} are the tunneling resistances when the magnetization directions of two FM layers are parallel and antiparallel, respectively. This relative change is expressed in terms of the spin polarization P_1 and P_2 of the two ferromagnetic electrodes using Jullière's model[75].

A tunnel magnetoresistance device provides the highest sensitivity among MR technologies. Commercial TMR ratios often exceed 100%, and CoFe(B)/MgO/CoFe(B) magnetic tunnel junctions have demonstrated values above 600% at room temperature and over 1000% at 10 K[76-79], attributed to coherent tunneling through crystalline MgO barriers. Common ferromagnetic materials include Fe, Ni, Co, CoFe, NiFe, and CoFeB[80-84], while insulating barriers include MgO, Al_2O_3, NiO, GdOx, Ga_2O_3, HfO_x, and ZrO_x[85-90]. Nowadays, CoFeB/MgO/CoFeB MTJ has been the most popular TMR sensor for spintronic devices. TMR sensors exhibit the lowest intrinsic noise among MR technologies, reaching sub-pT/√Hz at room temperature [91, 92]. The high resistance of the tunnel barrier also leads to lower power consumption compared with AMR and GMR. Thermal stability depends strongly on interface quality, atomic diffusion, and soft magnetic layer degradation. At the device level, many practical TMR sensors are specified to operate up to about 125 °C, beyond which temperature-induced drift and reliability concerns become significant. In contrast, the MTJ stack itself can remain

structurally robust at much higher temperatures. Ta-doped CoFeSiB soft layers can enhance thermal tolerance to 425 °C [93].

Despite the highest MR ratio, the lowest noise floor, superior signal-to-noise ratio, and reduced power consumption, TMR device requires highly controlled multilayer fabrication and high-quality interfaces, making the process technologically demanding. Thermal stability and long-term reliability remain critical considerations, particularly for operation in harsh environments.

Magnetoresistive sensors are increasingly deployed across mineral exploration platforms, including ground-based arrays for high-resolution near-surface profiling, UAV-mounted systems for rapid surveys over challenging terrain, and compact downhole tools for deep mineral mapping under elevated temperature and pressure conditions[54, 94, 95]. Among the different MR technologies, AMR sensors are particularly suitable for high-temperature and cost-sensitive applications due to their structural simplicity and thermal robustness. Giant magnetoresistance sensors provide improved sensitivity and wider dynamic range for medium-field detection, while tunneling magnetoresistance sensors offer the highest resolution and lowest noise density, making them promising for weak magnetic anomaly detection in compact airborne systems. Although MR sensors do not reach the ultimate sensitivity of quantum magnetometers, their solid-state robustness, compact size, scalability, and compatibility with microelectronic integration make them highly competitive for distributed, miniaturized, and field-deployable mineral exploration systems.

2.4 MEMS sensors

Microelectromechanical systems magnetic sensors represent a rapidly emerging class of devices that integrate miniaturized mechanical resonators with magnetic sensing mechanisms. By leveraging mechanical transduction, these sensors can amplify magnetic signals while maintaining small size, batch fabrication capability, CMOS compatibility, and versatile device configurations[96, 97].

Here, we focus specifically on MEMS magnetic sensors incorporating mechanically resonant structures, distinguishing them from devices that merely employ MEMS fabrication process without movable or resonant elements. Resonant MEMS magnetic sensors can be categorized into Lorentz-force, magnetostrictive, magnetoelectric, and magnetic torque-based devices, depending on the underlying magneto-mechanical coupling mechanism. Since limited research has been reported on MEMS-based magnetic torque sensors, they will not be discussed in detail in this review [98]. Silicon remains the dominant substrate due to its mature micromachining processes, CMOS compatibility, and low fabrication cost, although Si-based devices are generally limited in high-

temperature or chemically aggressive environments.

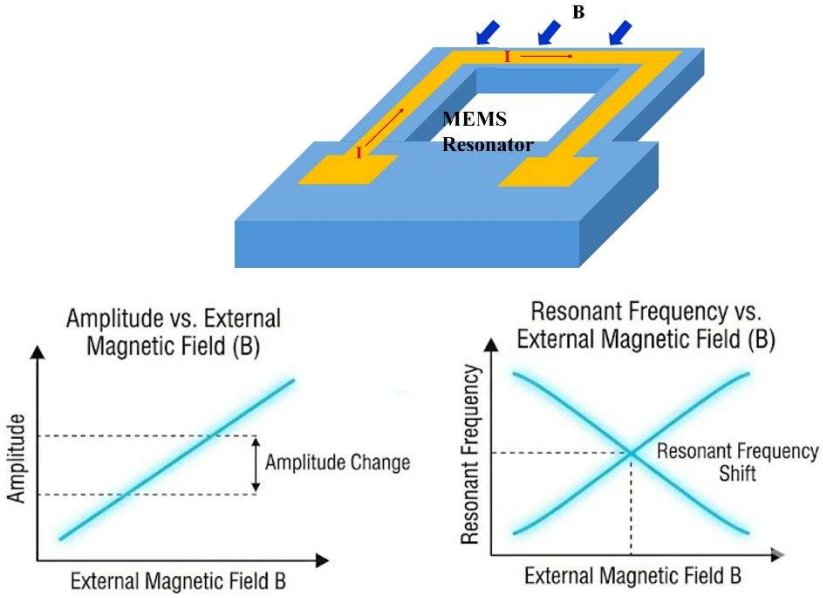

Figure 5 Schematic principle of a Lorentz force-based MEMS magnetic sensor. When a electric current (mostly AC) flows through the planar coil integrated onto the surface of the MEMS resonators (i.e. Si), under an external magnetic field **(B)**, the interaction between the current in the coil and the magnetic field generates an oscillating Lorentz Force perpendicular to both the current direction and the magnetic field lines, leading to the change of the vibrational amplitude or the frequency shift of the resonator. The resonator can be actuated by electrostatical or piezoelectric way.

The Lorentz-force MEMS magnetic (LFMM) sensor converts magnetic flux density into a mechanical deflection or vibration of a microfabricated structure, as shown in Figure 5. When an electrical current is driven through a suspended conductive beam or a metal trace on a MEMS resonator placed in an external magnetic field **B**, the structure experiences a Lorentz force given by

$$\mathbf{F} = I\,\mathbf{L} \times \mathbf{B}$$

where **L** is the effective current path vector. The resulting force induces a displacement or resonance frequency shift of the resonator. The mechanical motion is then transduced into an electrical output using capacitive, piezoresistive, piezoelectric, or optical readout schemes. In resonant implementations, the sensor is operated near its mechanical resonance to enhance sensitivity.

The key performance metrics of LFMM sensors include resonance frequency, quality

(Q) factor, responsivity, resolution, and power consumption. A high Q factor is generally desirable to maximize responsivity and improve magnetic resolution. A detectable field of 143 nT at 136.52 kHz was demonstrated for a seesaw resonator with a Q factor of 842 using piezoresistive readout [99]. By using capacitive readout schemes, a resolution of approximately 1 nT at 2.5 kHz within a 35 Hz bandwidth was achieved for the resonator with a Q factor around 700 [100]. The integration of a piezoelectric material on the resonator (e.g. AlN-on-Si) performed both on-chip actuation and sensing [101]. In many practical implementations, noise levels are on the order of μT/√Hz, primarily limited by current-induced thermal (Johnson) noise [102]. By optimizing the resonator dimensions and operating under vacuum to suppress air damping and enhance Q factors, the noise level approached nT/√Hz level [103]. Typical power consumption is on the order of milliwatts. Although resonance frequency and Q-factor stability were characterized up to approximately 190°C[103], there have been few demonstrations of high-temperature magnetic sensing using LFMM devices. An important advantage of this LFMM sensors is that no magnetic materials are required, thereby eliminating magnetic hysteresis effects.

The operation of magnetostrictive MEMS magnetic sensors results from the ΔE effect [104], as shown in Figure 6. When a ferromagnetic material is subjected to an external magnetic field, magnetic domain rotation and alignment occur, leading not only to magnetostriction (strain) but also to a variation in the material's effective Young's modulus. This magnetic-field-induced change in elastic modulus alters the mechanical stiffness of the resonator. Typically, a magnetostrictive thin film is deposited onto a mechanical resonator for magnetic sensing. Under an applied magnetic field, the effective Young's modulus E_{eff} of the multilayer structure changes, resulting in a shift in resonance frequency. The magnetic field is thus inferred from the frequency shift of the resonator. The direction and magnitude of the frequency shift depend on the stress state (tensile or compressive) and the magnetoelastic coupling of the material. Similar to LFMM devices operating in resonant modes, the sensitivity and frequency resolution of magnetostrictive sensors are also strongly dependent on the Q factor of the resonator.

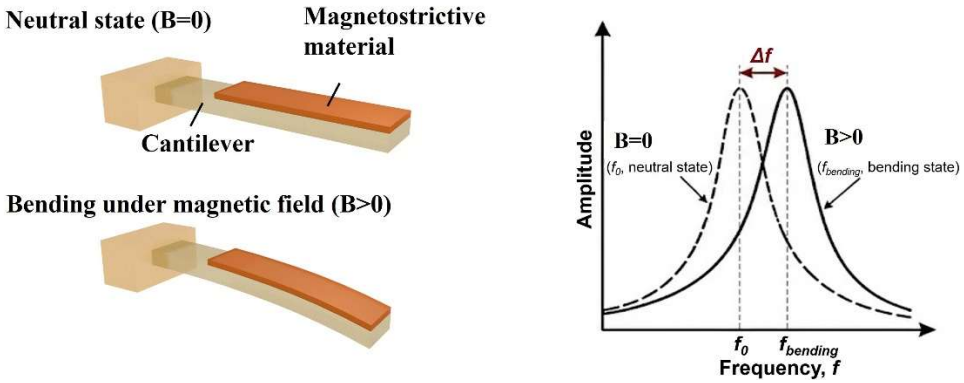

Figure 6 Principle of a resonant MEMS magnetic sensor using a magnetostrictive material/cantilever structure. Applying an external magnetic field (H>0) triggers the ΔE effect, altering the magnetic layer's elastic stiffness, which change the resonance frequency of the MEMS resonator. The measurable frequency shift reflects the magnetic field strength. The decrease or increase of the resonance frequency depends on the stress states (compressive or tensile).

The realization of high-temperature magnetostrictive MEMS sensors relies on the selection of the MEMS substrate and the magnetic material. Single-crystal diamond (SCD) is utilized as the ultimate mechanical resonator platform due to its outstanding mechanical strength, high thermal conductivity, chemical inertness, and exceptional intrinsic thermal stability[105-108]. On the other hand, FeGa exhibits a large magnetostriction coefficient and possesses a high Curie temperature above 650°C, making it highly resilient to thermal degradation[109]. Devices based on the FeGa/Ti/SCD structure maintain robust operation at high temperatures and magnetic noise levels of 10 nT/√Hz even at 500°C [110]. Additionally, all-electrical actuation and readout on-chip sensors based on FeGa/SCD MEMS were demonstrated, which is stable up to 300°C [111]. These results highlight the suitability of magnetostrictive MEMS sensors for high-temperature magnetic field detection. Additionally, the integration capability of SCD MEMS platforms enables simultaneous temperature and magnetic field sensing on the same chip, providing multifunctional sensing capability [112]. By integrating a piezoelectric layer with magnetostrictive material, piezoelectric readout can be achieved [113, 114]. These magnetoelectric sensors also show low noise levels of ~5.1 pT/√Hz at 1 Hz[113]. By using high-Curie ferroelectric materials, the operation temperature up to 350°C was demonstrated [115]. However, the direct deposition of piezoelectric material on diamond is quite difficult[116, 117]. The device structure and materials process need to be optimized if SCD is used as the mechanical resonator for high-temperature applications.

MEMS magnetic sensors have been evolving from proof-of-concept laboratory structures to increasingly integrated platforms. Advances in microfabrication have enabled improved resonator geometries, higher Q factors, and reduced mechanical damping[118]. Integration of on-chip actuation and readout, whether capacitive, piezoresistive, or piezoelectric, has enhanced system compactness and signal stability. Vacuum packaging techniques have further improved performance by minimizing air damping and increasing Q factors. In magnetostrictive systems, multilayer engineering and interface optimization have improved magnetoelastic coupling efficiency[110]. The transition from silicon-based platforms toward wide-bandgap semiconductors-based resonators marks a significant step toward high-temperature and harsh-environment operation.

MEMS magnetic sensors based on mechanical resonance provide signal amplification, improving sensitivity relative to purely electrical microscale sensors. Lorentz-force devices avoid magnetic hysteresis due to the absence of ferromagnetic cores. Magnetostrictive MEMS sensors, particularly those based on diamond substrates, exhibit strong potential for high-temperature and chemically aggressive environments. However, LFMM sensors require drive current, introducing thermal noise and limiting ultimate sensitivity. Their performance is strongly dependent on Q factor and environmental damping. High-temperature operation remains less explored for LFMM sensors. Magnetostrictive devices require ferromagnetic films, which may introduce magnetic nonlinearity or domain-related noise.

MEMS magnetic sensors offer promising opportunities for compact, low-power, and potentially high-temperature magnetic sensing. Lorentz-force MEMS devices are attractive for portable and UAV-based surveys due to their mechanical robustness and absence of magnetic hysteresis. Magnetostrictive MEMS sensors, especially those employing high-Curie temperature magnetic materials (e.g. FeGa films) on diamond resonators, demonstrate strong potential for deep-earth and high-temperature borehole applications.

While the performance of MEMS magnetic sensors requires much improvement when compared to high-end quantum magnetometers, ongoing efforts in resonator design, vacuum packaging, advanced materials, and integration technologies continue to enhance their overall capabilities. With further development, MEMS magnetic sensors are poised to complement conventional magnetometers by enabling distributed, miniaturized, and harsh-environment-compatible magnetic sensing platforms for both near-surface and deep mineral exploration.

3. Applications in mineral exploration

Magnetic sensors have long been a cornerstone of geophysical exploration due to their ability to detect variations in the Earth's magnetic field caused by the presence of ferromagnetic minerals, structural features, and lithological contrasts. Their non-destructive nature, combined with the low cost and fast mapping for large areas, makes them particularly valuable for both regional reconnaissance and detailed site-specific studies. In mineral exploration, magnetic sensors are applied across multiple scales and platforms, providing essential information for detecting ore deposits, delineating geological structures, and guiding drilling programs.

The most important magnetically susceptible mineral is magnetite (Fe_3O_4), and to a lesser extent, ilmenite ($FeTiO_3$) and pyrrhotite ($Fe_{1-x}S$). Magnetometric surveys can be used for the direct detection of ore, or for the indirect detection of geologic features associated with ore deposits. By measuring the spatial distribution, amplitude, and gradient of magnetic anomalies, geophysicists can infer the presence, geometry, and concentration of ore bodies before drilling, reducing exploration costs and increasing targeting efficiency.

Magnetic sensors are also used for mapping geological structures that control mineralization[119]. Faults, shear zones, dike swarms, and lithological boundaries often produce magnetic contrasts due to variations in rock composition and magnetite content[120]. High-resolution surveys using vector magnetometers or magnetic sensor arrays can delineate these structures, revealing the orientation, extent, and connectivity of potential mineralizing pathways[4]. For instance, in layered mafic intrusions hosting Ni–Cu sulfide deposits, detailed magnetic mapping can identify the spatial distribution of magnetite-bearing cumulate layers and associated feeder channels[121-123]. Similarly, hydrothermal systems such as Iron oxide copper gold (IOCG) deposits or porphyry Cu-Au deposits often exhibit magnetic lows or highs reflecting magnetite destruction or emplacement[124]. Because minerals like magnetite, hematite, and pyrrhotite are commonly associated with hydrothermal alteration, mapping these anomalies infers that a mineralizing hydrothermal event has affected the host rocks[125]. This structural and lithological information is critical for drilling targeting and 3D geological modeling[125].

Magnetic sensors are deployed across multiple platforms depending on exploration objectives, survey scale, and terrain accessibility. Magnetic surveys are generally classified into three main operational domains: land-based (surface and deep underground), airborne, and marine surveys[126, 127].

Land surveys provide the highest spatial resolution and are categorized into surface (ground-based) and deep subsurface (borehole) applications. Ground-based magnetic

surveys can be conducted using portable magnetic sensors. These surveys provide excellent control over sensor orientation and are particularly valuable in rugged terrain, densely vegetated regions, or urban environments, enabling high-resolution mapping of near-surface magnetic anomalies and structurally controlled mineralized zones. Deep or borehole magnetic surveys overcome the limitations of surface masking by overburden by placing sensors directly within boreholes or underground mines, which provide important constraints on geometry, magnetization, and depth of deep ore bodies. These measurements often require magnetic sensors capable of operating under elevated temperatures and strong geothermal gradients. Emerging high-temperature magnetic sensors based on wide-bandgap semiconductors, including MEMS and Hall devices, are being explored for such applications.

Airborne magnetic surveys are a widely used form of magnetic exploration due to their rapid data acquisition, cost effectiveness, and capability to cover large and remote areas. They enable efficient mapping of regional magnetic anomalies and geological structures, particularly in terrains that are difficult or inaccessible for ground surveys[128]. Airborne magnetic surveys are typically conducted using fixed-wing aircraft, helicopters, or UAVs. In recent years, compact magnetic sensors have attracted increasing attention for airborne and UAV platforms due to their small size, low power consumption, and potential for operation in harsh environments. These systems enable rapid and uniform coverage over large mining regions, facilitating the mapping of regional lithological variations, major faults, and intrusive complexes.

For offshore mineral exploration, magnetic measurements are taken at ocean depths or across the sea surface [129, 130]. In these surveys, the magnetic sensor is towed in a specialized housing known as a “fish”. The magnetometer “fish” is typically towed several ship lengths behind the survey vessel in order to minimize magnetic interference generated by the ship itself[131]. Marine surveys expand the reach of magnetic sensing to underwater ore deposits and are often conducted alongside other continuous geophysical profiling methods[132, 133].

The combination of various magnetic sensors enables the detection of both near-surface and deeply buried mineral deposits, making magnetic sensing a central tool in modern mineral exploration. Currently, sensing datasets have become massive in volume, and geological information is increasingly complex in its dimensionality, noise levels, and non-linearity, especially when multi-component sensing is adopted. Traditional processing methods have been facing difficulties in handling such big data. Machine learning (ML) techniques, including support vector machines, random forests, and deep neural networks[134-136], have emerged as powerful and efficient data-driven paradigms

for magnetic data interpretation, improving the accuracy of mineral exploration, classification, and predictive targeting [137-139]. Recently, Tiny Machine Learning (TinyML) has attracted attention for predicting real-time terrestrial magnetic perturbations directly [140].

4. Summary and outlook

In summary, magnetic sensors provide non-invasive, rapid, and cost-effective information on subsurface geology, enabling exploration geophysicists to delineate ore bodies, reconstruct structural frameworks, and optimize drilling campaigns. A variety of high-temperature magnetic sensor technologies are employed in magnetic sensing systems, including fluxgate, MR, Hall-effect, and MEMS-based devices, each providing unique performance characteristics in terms of sensitivity, size, power consumption, and environmental tolerance. In Table 1, we summarize the basic properties of the magnetic sensors based on the four types of magnetometers. Diamond NV-center quantum magnetometers offer a theoretical magnetic sensitivity at room temperature comparable to SQUIDs and have experimentally achieved pT-level sensitivity as well as nanoscale spatial resolution[141, 142]. However, their application in mineral exploration has yet to be demonstrated. For the properties of other types of magnetic sensors, one can find in reported literature [143, 144].

While these miniaturized magnetic sensors reviewed in this paper have revolutionized multi-platform mineral exploration, challenges remain in bridging the performance gap with high-end quantum magnetometers. Currently, traditional high-sensitivity quantum devices remain constrained by complex cooling requirements, limiting their field deployment. Conversely, solid-state sensors excel in SWaP-C (Size, Weight, Power, and Cost) metrics but often face trade-offs involving limited sensitivity, increased noise floors, or restricted dynamic ranges. Addressing this balance is critical for advancing autonomous magnetic survey systems, particularly in remote regions or harsh environments.

Adaptability to extreme environments is another critical area of future research. As exploration targets shift deeper, sensors will face intense geothermal gradients, high pressures, and corrosive environments. Transitioning from conventional silicon platforms to robust wide-bandgap semiconductors and advanced MEMS architectures will be essential to expanding depth penetration and reliability.

Table 1 Performance comparison of high-temperature magnetic sensors

Sensor Category	Specific Type	Materials	Noise level@1Hz	Field range	Operation temperatures
Fluxgate	**Single rod, dual core, ring core, race-track**	Soft magnetic cores like NiFe alloys, CoFeMoSiB, and nanocrystalline materials	~ pT/√Hz	100 pT-100 mT	250°C.
Hall effect	**Planar, vertical**	Silicon, InSb, InAs, GaN, SiC, 2D materials (Graphene, MoS_2)	>100nT/√Hz	μT-T	400 °C (GaN) 500 °C (SiC)
Magnetoresistive	**AMR**	3d transition metals (Fe, Ni, Co) and alloys (e.g., permalloy).	100 pT-10 nT/√Hz	μT- mT	225°C
	GMR	Heterostructures of ferromagnetic layers (Co, CoFe, NiFe) and nonmagnetic spacers (Cu, Cr, Ag). Pinning layers (IrMn, PtMn, NiMn etc) stabilize the layers.	Sub-nT-10 nT/√Hz	μT-mT	120°C
	TMR	Similar to GMR but utilizes an ultra-thin insulating barrier (MgO, Al_2O_3, etc.).	Sub-pT-10 nT/√Hz	pT-mT	125°C
MEMS	**Lorentz-force**	Silicon, SiC, diamond SU-8, polyimide as resonators, Al, Cu, Pt, Au as the conductive wires	nT- μT/√Hz	nT-T	190°C.
	Magnetostrictive	Silicon, diamond as the resonators paired with magnetostrictive films like FeGa. Piezoelectric materials are also included for electric readout in many cases.	pT~10 nT/√Hz	pT–mT	500°C

Furthermore, the future of mineral exploration lies in multi-modal integration and intelligent data processing. The co-deployment of compact magnetic sensors alongside temperature, gravity, electromagnetic, and seismic methods will enable comprehensive subsurface characterization. Coupled with advanced machine learning algorithms to handle massive, noisy, and non-linear multi-component datasets, these integrated arrays will drive the next generation of accurate, real-time predictive targeting for deeply buried mineral deposits.

Declaration of Competing Interest

The authors declare that they have no known competing financial interests or personal relationships that could have appeared to influence the work reported in this paper.

Acknowledgements

This work was supported by JSPS KAKENHI (Grant Number 25KF0081 and 24H00287) and ARIM (JPMXP1225NM5307) sponsored by the Ministry of Education, Culture, Sports, and Technology (MEXT) of Japan.

References

[1] E. C. Ferré, I. Kupenko, F. Martín-Hernández, D. Ravat, and C. Sanchez-Valle, "Magnetic sources in the Earth's mantle," *Nature Reviews Earth & Environment,* vol. 2, no. 1, pp. 59-69, 2021/01/01 2021, doi: 10.1038/s43017-020-00107-x.

[2] "Magnetization of Earth materials," in *Gravity and Magnetic Exploration: Principles, Practices, and Applications*, W. J. Hinze, R. R. B. von Frese, and A. H. Saad Eds. Cambridge: Cambridge University Press, 2013, pp. 252-275.

[3] A. Zohdy, G. Eaton, and D. Mabey, "Application of surface geophysics to ground-water investigations," in "Techniques of Water-Resources Investigations," Report 02-D1, 1974. [Online]. Available: https://pubs.usgs.gov/publication/twri02D1

[4] W. M. Telford, L. P. Geldart, and R. E. Sheriff, *Applied Geophysics*. Cambridge University Press, 1990.

[5] H. Zhou, Z. Qiao, P. Yuan, Y. Huang, L. Zhu, C. Yang, L. Wang, L. Zheng, Y. Wang, B. Wu, and Q. Lin, "Research on the application of unmanned aerial vehicle aeromagnetic measurement based on rubidium optical pump magnetometer," *Scientific Reports,* vol. 16, no. 1, p. 4599, 2026/01/09 2026, doi: 10.1038/s41598-025-34622-y.

[6] R. Stolz, M. Schiffler, M. Becken, A. Thiede, M. Schneider, G. Chubak, P. Marsden, A. B. Bergshjorth, M. Schaefer, and O. Terblanche, "SQUIDs for magnetic and electromagnetic methods in mineral exploration," *Mineral Economics,* vol. 35, no. 3, pp. 467-494, 2022/12/01 2022, doi: 10.1007/s13563-022-00333-3.

[7] P. Ripka, "Advances in fluxgate sensors," *Sensors and Actuators A: Physical,* vol. 106, no. 1, pp. 8-14, 2003/09/15/ 2003, doi: https://doi.org/10.1016/S0924-4247(03)00094-3.

[8] V. S. Luong, M. Le, and V. P. Quang, "Fluxgate-Based Displacement Sensor Design," *Journal of Superconductivity and Novel Magnetism,* vol. 36, no. 7, pp. 1767-1775, 2023/09/01 2023, doi: 10.1007/s10948-023-06620-6.

[9] R. Pavel, "Magnetic Sensors and Magnetometers," *Measurement Science and Technology,* vol. 13, no. 4, p. 645, 2002/04/01 2002, doi: 10.1088/0957-0233/13/4/707.

[10] T. Dyer, P. F. Griffin, and E. Riis, "Single-board low-noise fluxgate magnetometer," *Journal of Applied Physics,* vol. 135, no. 3, 2024, doi: 10.1063/5.0175418.

[11] P. Ripka, F. Primdahl, O. V. Nielsen, J. R. Petersen, and A. Ranta, "A.c. magnetic-field measurement using the fluxgate," *Sensors and Actuators A: Physical,* vol. 46, no. 1, pp. 307-311, 1995/01/01/ 1995, doi: https://doi.org/10.1016/0924-4247(94)00911-Z.

[12] C. Hinnrichs, C. Pels, and M. Schilling, "Noise and linearity of a fluxgate magnetometer in racetrack geometry," *Journal of Applied Physics,* vol. 87, no. 9, pp. 7085-7087, 2000, doi: 10.1063/1.372939.

[13] B. Yan, W. Zhu, X. Zhuang, Z. Lu, and G. Fang, "Development of a High-Temperature Co-Fe-Si-

B Amorphous Wire Fluxgate Magnetometer for Downhole Attitude Measurement in MWD Systems at Temperatures up to 175 °C," *Sensors,* vol. 25, no. 19, p. 5972, 2025. [Online]. Available: https://www.mdpi.com/1424-8220/25/19/5972.

[14] D. Rühmer, S. Bögeholz, F. Ludwig, and M. Schilling, "Vector fluxgate magnetometer for high operation temperatures up to 250°C," *Sensors and Actuators A: Physical,* vol. 228, pp. 118-124, 2015/06/01/ 2015, doi: https://doi.org/10.1016/j.sna.2015.03.004.

[15] P. Yu, G. Huang, J. Jiao, L. Zhou, Y. Zhao, P. Lu, L. Li, and S. Shi, "A Quadrotor UAV Aeromagnetic Compensation Method Based on Time–Frequency Joint Representation Neural Network and Its Application in Mineral Exploration," *Sensors,* vol. 25, no. 18, p. 5774, 2025. [Online]. Available: https://www.mdpi.com/1424-8220/25/18/5774.

[16] P. Lipovský, K. Draganová, J. Novotňák, Z. Szőke, and M. Fiľko, "Indoor Mapping of Magnetic Fields Using UAV Equipped with Fluxgate Magnetometer," *Sensors,* vol. 21, no. 12, p. 4191, 2021. [Online]. Available: https://www.mdpi.com/1424-8220/21/12/4191.

[17] E. H. Hall, "On a New Action of the Magnet on Electric Currents," *American Journal of Mathematics,* vol. 2, no. 3, pp. 287-292, 1879, doi: 10.2307/2369245.

[18] A. Karsenty, "A Comprehensive Review of Integrated Hall Effects in Macro-, Micro-, Nanoscales, and Quantum Devices," *Sensors,* vol. 20, no. 15, p. 4163, 2020. [Online]. Available: https://www.mdpi.com/1424-8220/20/15/4163.

[19] M. M. Parmar, H. Saren, and P. Das, "Fabrication and Characterization of InAs/AlSb based Magnetic Hall Sensors," in *2020 5th IEEE International Conference on Emerging Electronics (ICEE)*, 26-28 Nov. 2020 2020, pp. 1-4, doi: 10.1109/ICEE50728.2020.9776959.

[20] M. Oszwałldowski, "Hall sensors based on heavily doped n-InSb thin films," *Sensors and Actuators A: Physical,* vol. 68, no. 1, pp. 234-237, 1998/06/15/ 1998, doi: https://doi.org/10.1016/S0924-4247(97)01779-2.

[21] M. Morvic and J. Betko, "Planar Hall effect in Hall sensors made from InP/InGaAs heterostructure," *Sensors and Actuators A: Physical,* vol. 120, no. 1, pp. 130-133, 2005/04/29/ 2005, doi: https://doi.org/10.1016/j.sna.2004.11.030.

[22] R. G. Mani, "Dual Hall effects in inhomogeneous doubly connected GaAs/AlGaAs heterostructure devices," *Applied Physics Letters,* vol. 70, no. 21, pp. 2879-2881, 1997, doi: 10.1063/1.119029.

[23] H. Sghaier, L. Sfaxi, L. Bouzaïene, and H. Maaref, "Sensitivity enhancement of AlGaAs/GaAs heterojunction-based Hall sensor designed for low magnetic field measurements," *Sensors and Actuators A: Physical,* vol. 113, no. 2, pp. 147-150, 2004/07/05/ 2004, doi: https://doi.org/10.1016/j.sna.2004.02.008.

[24] J.-L. Robert, S. Contreras, J. Camassel, J. Pernot, E. Neyret, L. Di Cioccio, and T. Billon, "4H-SiC: a material for high temperature Hall sensor," *Sensors and Actuators A: Physical,* vol. 97-98, pp. 27-32, 2002/04/01/ 2002, doi: https://doi.org/10.1016/S0924-4247(01)00812-3.

[25] J.-L. Robert, S. Contreras, J. Camassel, J. Pernot, E. Neyret, L. Di Cioccio, and T. Billon, "Investigation of 4H-SiC as a New Material for Hall or Temperature Sensors Working up to 500 °C," in *Transducers '01 Eurosensors XV*, Berlin, Heidelberg, E. Obermeier, Ed., 2001// 2001: Springer Berlin Heidelberg, pp. 986-989.

[26] V. Marsic, S. Faramehr, I. Maini, D. A. J. Moran, and P. Igic, "Study of GaN Hall Effect Magnetic Sensors," *IEEE Access,* vol. 13, pp. 25622-25636, 2025, doi: 10.1109/ACCESS.2025.3539435.

[27] V. Marsic, S. Faramehr, J. Fleming, R. Bhagat, and P. Igic, "Understanding the limits of a hall sensor sensitivity for integration on a GaN power transistor chip: experiments with market available components," in *12th International Conference on Power Electronics, Machines and Drives (PEMD 2023)*, 23-24 Oct. 2023 2023, vol. 2023, pp. 350-356, doi: 10.1049/icp.2023.2022.

[28] S. Koide, H. Takahashi, A. Abderrahmane, I. Shibasaki, and A. Sandhu, "High Temperature Hall sensors using AlGaN/GaN HEMT Structures," *Journal of Physics: Conference Series,* vol. 352, no. 1, p. 012009, 2012/03/05 2012, doi: 10.1088/1742-6596/352/1/012009.

[29] K. Ma, H. Huang, N. Sun, N. Ding, Q. Zuo, W. Shan, L. Zhang, G. Lv, J. Dai, and D. Fu, "GaN-based shallow-trench vertical Hall devices," *Applied Physics Letters,* vol. 126, no. 3, 2025, doi: 10.1063/5.0250222.

[30] S. Kumar, R. Muralidharan, and G. Narayanan, "Hall-effect sensors based on AlGaN/GaN heterojunctions on Si substrates for a wide temperature range," *IET Circuits, Devices & Systems,* vol. 15, no. 8, pp. 772-786, 2021, doi: https://doi.org/10.1049/cds2.12067.

[31] L. Bouguen, L. Konczewicz, S. Contreras, B. Jouault, J. Camassel, and Y. Cordier, "High temperature behaviour of AlGaN/AlN/GaN Hall-FET sensors," *Materials Science and Engineering: B,* vol. 165, no. 1, pp. 1-4, 2009/11/25/ 2009, doi: https://doi.org/10.1016/j.mseb.2008.11.041.

[32] A. Kumar, R. Muralidharan, and G. Narayanan, "Comparison of GaN and GaAs based Hall Magnetic Sensor for Power Applications," in *2022 IEEE International Symposium on Smart Electronic Systems (iSES)*, 18-22 Dec. 2022 2022, pp. 316-320, doi: 10.1109/iSES54909.2022.00071.

[33] T. zhenyu, T. Xiaoyan, Z. Yimeng, Z. Pu, S. Yuyin, and Z. Yuming, "4H-SiC integrated circuits for high-temperature applications," *Journal of Crystal Growth,* vol. 605, p. 127060, 2023/03/01/ 2023, doi: https://doi.org/10.1016/j.jcrysgro.2022.127060.

[34] C. Unger and M. Pfost, "Thermal Stability of SiC-MOSFETs at High Temperatures," *IEEE Transactions on Electron Devices,* vol. 66, no. 11, pp. 4666-4672, 2019, doi: 10.1109/TED.2019.2942011.

[35] H. Okeil, T. Erlbacher, and G. Wachutka, "Very High Temperature Hall Sensors in a Wafer-Scale 4H-SiC Technology," *Advanced Materials Technologies,* vol. 10, no. 1, p. 2400046, 2025, doi: https://doi.org/10.1002/admt.202400046.

[36] B. A. Kaidarova, W. Liu, L. Swanepoel, A. Almansouri, N. R. Geraldi, C. M. Duarte, and J. Kosel, "Flexible Hall sensor made of laser-scribed graphene," *npj Flexible Electronics,* vol. 5, no. 1, p. 2, 2021/02/15 2021, doi: 10.1038/s41528-021-00100-4.

[37] T. Ciuk, O. Petruk, A. Kowalik, I. Jozwik, A. Rychter, J. Szmidt, and W. Strupinski, "Low-noise epitaxial graphene on SiC Hall effect element for commercial applications," *Applied Physics Letters,* vol. 108, no. 22, 2016, doi: 10.1063/1.4953258.

[38] C. Jiang, A. Rasmita, H. Ma, Q. Tan, Z. Zhang, Z. Huang, S. Lai, N. Wang, S. Liu, X. Liu, T. Yu, Q. Xiong, and W.-b. Gao, "A room-temperature gate-tunable bipolar valley Hall effect in molybdenum disulfide/tungsten diselenide heterostructures," *Nature Electronics,* vol. 5, no. 1, pp. 23-27, 2022/01/01 2022, doi: 10.1038/s41928-021-00686-7.

[39] S. Guo, "Simulations of residual offset of Five-Contact vertical Hall devices with slim waist," *Solid-State Electronics,* vol. 178, p. 107986, 2021/04/01/ 2021, doi: https://doi.org/10.1016/j.sse.2021.107986.

[40] C. Sander, M.-C. Vecchi, M. Cornils, and O. Paul, "From Three-Contact Vertical Hall Elements to Symmetrized Vertical Hall Sensors with Low Offset," *Sensors and Actuators A: Physical,* vol. 240, pp. 92-102, 2016/04/01/ 2016, doi: https://doi.org/10.1016/j.sna.2016.01.040.

[41] T. Zhou, J. Cai, and X. Zhu, "An Advanced Hall Element Array-Based Device for High-Resolution Magnetic Field Mapping," *Sensors,* vol. 24, no. 12, p. 3773, 2024. [Online]. Available: https://www.mdpi.com/1424-8220/24/12/3773.

[42] H. Fan, J. Zhang, S. Zuo, Q. Hu, Q. Feng, and H. Heidari, "A CMOS Hall sensor modeling with readout circuitry and microcontroller processing for magnetic detection," *Review of Scientific Instruments,* vol. 92, no. 3, 2021, doi: 10.1063/5.0038295.

[43] F. J. P. v. Mourik, S. Pan, K. M. Dowling, and K. A. A. Makinwa, "27.2 A Voltage-Biased CMOS Hall Sensor with 1.0μT(3 σ) Offset and a60nT/ $Hz^{1/2}$ Noise-Floor," in *2025 IEEE International Solid-State Circuits Conference (ISSCC)*, 16-20 Feb. 2025 2025, vol. 68, pp. 1-3, doi: 10.1109/ISSCC49661.2025.10904555.

[44] F. Accomando and G. Florio, "Applicability of Small and Low-Cost Magnetic Sensors to Geophysical Exploration," (in eng), *Sensors (Basel),* vol. 24, no. 21, Oct 31 2024, doi: 10.3390/s24217047.

[45] J. Velev, R. F. Sabirianov, S. S. Jaswal, and E. Y. Tsymbal, "Ballistic Anisotropic Magnetoresistance," *Physical Review Letters,* vol. 94, no. 12, p. 127203, 03/30/ 2005, doi: 10.1103/PhysRevLett.94.127203.

[46] S. Mostufa, S. Liang, V. K. Chugh, J.-P. Wang, and K. Wu, "Spintronic devices for biomedical applications," *npj Spintronics,* vol. 2, no. 1, p. 26, 2024/07/02 2024, doi: 10.1038/s44306-024-00031-6.

[47] P. Ritzinger and K. Výborný, "Anisotropic magnetoresistance: materials, models and

applications," *Royal Society Open Science,* vol. 10, no. 10, 2023, doi: 10.1098/rsos.230564.

[48] S. Lendínez, T. Polakovic, J. Ding, M. B. Jungfleisch, J. Pearson, A. Hoffmann, and V. Novosad, "Temperature-dependent anisotropic magnetoresistance and spin-torque-driven vortex dynamics in a single microdisk," *Journal of Applied Physics,* vol. 127, no. 24, 2020, doi: 10.1063/5.0006557.

[49] S. Wang, T. Gao, C. Wang, and J. He, "Studies of anisotropic magnetoresistance and magnetic property of Ni81Fe19 ultra-thin films with the lower base vacuum," *Journal of Alloys and Compounds,* vol. 554, pp. 405-407, 2013/03/25/ 2013, doi: https://doi.org/10.1016/j.jallcom.2012.12.004.

[50] R. Zhu, L. Yu, X. Ma, Q. Guo, X. Xu, C. Shi, F. Meng, B. Li, G. Yu, and C. Feng, "Orbit-Engineered Anisotropic Magnetoresistive Effect for Constructing a Magnetic Sensor with Ultrahigh Sensitivity," *ACS Applied Materials & Interfaces,* vol. 14, no. 7, pp. 9917-9924, 2022/02/23 2022, doi: 10.1021/acsami.1c24832.

[51] S. P. V, U. P. Borole, R. Kadam, J. Khan, H. C. Barshilia, and P. Chowdhury, "A novel AMR based angle sensor with reduced harmonic errors for automotive applications," *Sensors and Actuators A: Physical,* vol. 324, p. 112573, 2021/06/15/ 2021, doi: https://doi.org/10.1016/j.sna.2021.112573.

[52] T. McGuire and R. Potter, "Anisotropic magnetoresistance in ferromagnetic 3d alloys," *IEEE Transactions on Magnetics,* vol. 11, no. 4, pp. 1018-1038, 1975, doi: 10.1109/TMAG.1975.1058782.

[53] H. Nagura, K. Saito, K. Takanashi, and H. Fujimori, "Influence of third elements on the anisotropic magnetoresistance in permalloy films," *Journal of Magnetism and Magnetic Materials,* vol. 212, no. 1, pp. 53-58, 2000/03/01/ 2000, doi: https://doi.org/10.1016/S0304-8853(99)00784-2.

[54] V. S. Shevtsov and P. A. Polyakov, "The influence of inhomogeneity in the distribution of electric current and magnetization on the characteristics of a barber-pole magnetic sensor," *Sensors and Actuators A: Physical,* vol. 393, p. 116808, 2025/10/16/ 2025, doi: https://doi.org/10.1016/j.sna.2025.116808.

[55] B. B. Pant, L. Withanawasam, M. Bohlinger, M. Larson, and B. W. Ohme, "High Temperature Anisotropic Magnetoresistive (AMR) Sensors," *Additional Conferences (Device Packaging, HiTEC, HiTEN, and CICMT),* vol. 2015, no. HiTEN, pp. 000236-000243, 2015, doi: 10.4071/HiTEN-Session7-Paper7_1.

[56] F. Qiu, J. Wang, Y. Zhang, G. Yang, and C. Weng, "Resolution limit of anisotropic magnetoresistance(AMR) based vector magnetometer," *Sensors and Actuators A: Physical,* vol. 280, pp. 61-67, 2018/09/01/ 2018, doi: https://doi.org/10.1016/j.sna.2018.07.031.

[57] F. Accomando and G. Florio, "Applicability of Small and Low-Cost Magnetic Sensors to Geophysical Exploration," *Sensors,* vol. 24, no. 21, p. 7047, 2024. [Online]. Available: https://www.mdpi.com/1424-8220/24/21/7047.

[58] J. Lenz and S. Edelstein, "Magnetic sensors and their applications," *IEEE Sensors Journal,* vol. 6, no. 3, pp. 631-649, 2006, doi: 10.1109/JSEN.2006.874493.

[59] G. Binasch, P. Grünberg, F. Saurenbach, and W. Zinn, "Enhanced magnetoresistance in layered magnetic structures with antiferromagnetic interlayer exchange," *Physical Review B,* vol. 39, no. 7, pp. 4828-4830, 03/01/ 1989, doi: 10.1103/PhysRevB.39.4828.

[60] M. N. Baibich, J. M. Broto, A. Fert, F. N. Van Dau, F. Petroff, P. Etienne, G. Creuzet, A. Friederich, and J. Chazelas, "Giant Magnetoresistance of (001)Fe/(001)Cr Magnetic Superlattices," *Physical Review Letters,* vol. 61, no. 21, pp. 2472-2475, 11/21/ 1988, doi: 10.1103/PhysRevLett.61.2472.

[61] S. M. Thompson, "The discovery, development and future of GMR: The Nobel Prize 2007," *Journal of Physics D: Applied Physics,* vol. 41, no. 9, p. 093001, 2008/03/28 2008, doi: 10.1088/0022-3727/41/9/093001.

[62] A. Fert, "Nobel Lecture: Origin, development, and future of spintronics," *Reviews of Modern Physics,* vol. 80, no. 4, pp. 1517-1530, 12/17/ 2008, doi: 10.1103/RevModPhys.80.1517.

[63] H. N. Fuke, K. Saito, Y. Kamiguchi, H. Iwasaki, and M. Sahashi, "Spin-valve giant magnetoresistive films with antiferromagnetic Ir-Mn layers," *Journal of Applied Physics,* vol. 81, no. 8, pp. 4004-4006, 1997, doi: 10.1063/1.364920.

[64] M. J. Kim, H. J. Kim, K. Y. Kim, S. H. Jang, and T. Kang, "The annealing effect on GMR properties of PtMn-based spin valve," *Journal of Magnetism and Magnetic Materials,* vol. 239, no. 1, pp. 195-197, 2002/02/01/ 2002, doi: https://doi.org/10.1016/S0304-8853(01)00554-6.

[65] C. Feng, Y. Li, L. Wang, Y. Cao, M. Yao, F. Meng, F. Yang, B. Li, K. Wang, and G. Yu, "Giant Strain Control of Antiferromagnetic Moment in Metallic FeMn by Tuning Exchange Spring Structure," *Advanced Functional Materials,* vol. 30, no. 14, p. 1909708, 2020, doi: https://doi.org/10.1002/adfm.201909708.

[66] E. Heppell, F. Maccherozzi, L. S. I. Veiga, S. Langridge, G. van der Laan, T. Hesjedal, and D. Backes, "Handle on the antiferromagnetic spin structure of NiO using a ferromagnetic adlayer," *Physical Review Materials,* vol. 9, no. 1, p. 014408, 01/27/ 2025, doi: 10.1103/PhysRevMaterials.9.014408.

[67] J. Q. Xiao, J. S. Jiang, and C. L. Chien, "Giant magnetoresistance in the granular Co-Ag system," *Physical Review B,* vol. 46, no. 14, pp. 9266-9269, 10/01/ 1992, doi: 10.1103/PhysRevB.46.9266.

[68] J. Q. Xiao, J. S. Jiang, and C. L. Chien, "Giant magnetoresistive properties in granular transition metals," *IEEE Transactions on Magnetics,* vol. 29, no. 6, pp. 2688-2693, 1993, doi: 10.1109/20.280939.

[69] S. Arana, E. Castano, and F. J. Gracia, "High temperature circular position sensor based on a giant magnetoresistance nanogranular Ag/sub x/Co/sub 1-x/ alloy," *IEEE Sensors Journal,* vol. 4, no. 2, pp. 221-225, 2004, doi: 10.1109/JSEN.2004.823682.

[70] G. Anderson, Y. Huai, and L. Miloslavsky, "Spin-Valve GMR Films Based on Antiferromagnetic

NiMn," *MRS Proceedings,* vol. 562, p. 45, 1999, Art no. 45, doi: 10.1557/PROC-562-45.

[71] K. Wu, D. Su, R. Saha, and J.-P. Wang, "Giant Magnetoresistance (GMR) Materials and Devices for Biomedical and Industrial Applications," in *Spintronics*, 2022, pp. 3-49.

[72] J. Zhang, Z. Jin, G. Chen, and J. Chen, "An ultrathin, rapidly fabricated, flexible giant magnetoresistive electronic skin," *Microsystems & Nanoengineering,* vol. 10, no. 1, p. 109, 2024/08/12 2024, doi: 10.1038/s41378-024-00716-2.

[73] A. Guedes, R. Macedo, G. Jaramillo, S. Cardoso, P. P. Freitas, and D. A. Horsley, "Hybrid GMR Sensor Detecting 950 pT/sqrt(Hz) at 1 Hz and Room Temperature," (in eng), *Sensors (Basel),* vol. 18, no. 3, Mar 6 2018, doi: 10.3390/s18030790.

[74] R. R. Sihombing, T. Scheike, J. Uzuhashi, H. Yasufuku, T. Ohkubo, Z. Wen, S. Mitani, and H. Sukegawa, "High entropy oxide epitaxial films with interface perpendicular magnetic anisotropy and tunnel magnetoresistance effect toward spintronic applications," *Materials Today,* vol. 88, pp. 12-23, 2025/09/01/ 2025, doi: https://doi.org/10.1016/j.mattod.2025.06.025.

[75] M. Julliere, "Tunneling between ferromagnetic films," *Physics Letters A,* vol. 54, no. 3, pp. 225-226, 1975/09/08/ 1975, doi: https://doi.org/10.1016/0375-9601(75)90174-7.

[76] J. Igarashi, B. Jinnai, K. Watanabe, T. Shinoda, T. Funatsu, H. Sato, S. Fukami, and H. Ohno, "Single-nanometer CoFeB/MgO magnetic tunnel junctions with high-retention and high-speed capabilities," *npj Spintronics,* vol. 2, no. 1, p. 1, 2024/01/04 2024, doi: 10.1038/s44306-023-00003-2.

[77] S. Yuasa, R. Matsumoto, A. Fukushima, H. Kubota, T. Nagahama, D. D. Djayaprawira, K. Tsunekawa, H. Maehara, Y. Nagamine, M. Nagai, S. Yamagata, Y. Suzuki, M. Mizuguchi, A. M. Deac, and K. Ando, "Giant tunneling magnetoresistance in MgO-based magnetic tunnel junctions and its industrial applications," in *2006 IEEE Nanotechnology Materials and Devices Conference*, 22-25 Oct. 2006 2006, vol. 1, pp. 186-187, doi: 10.1109/NMDC.2006.4388737.

[78] S. Ikeda, J. Hayakawa, Y. Ashizawa, Y. M. Lee, K. Miura, H. Hasegawa, M. Tsunoda, F. Matsukura, and H. Ohno, "Tunnel magnetoresistance of 604% at 300K by suppression of Ta diffusion in CoFeB/MgO/CoFeB pseudo-spin-valves annealed at high temperature," *Applied Physics Letters,* vol. 93, no. 8, 2008, doi: 10.1063/1.2976435.

[79] T. Scheike, Z. Wen, H. Sukegawa, and S. Mitani, "631% room temperature tunnel magnetoresistance with large oscillation effect in CoFe/MgO/CoFe(001) junctions," *Applied Physics Letters,* vol. 122, no. 11, 2023, doi: 10.1063/5.0145873.

[80] L. N. Jiang, B. Y. Chi, and X. F. Han, "Quantum-well resonance enhanced tunneling magnetoresistance effect in magnetic tunnel junctions with oxidized interface," *Physical Review B,* vol. 111, no. 22, p. 224422, 06/20/ 2025, doi: 10.1103/39xc-2f3m.

[81] B. G. Park, T. D. Lee, T. H. Lee, C. G. Kim, and C. O. Kim, "Magnetic tunnel junctions with Hf oxide and modified Hf oxide tunnel barriers," *Journal of Applied Physics,* vol. 93, no. 10, pp.

6423-6425, 2003, doi: 10.1063/1.1540141.

[82] A. Khanas, C. Hebert, D. Hrabovsky, L. Becerra, and N. Jedrecy, "Multilevel magnetoresistance states in La0.7Sr0.3MnO3/BaTiO3/La0.7Sr0.3MnO3 heterostructure grown on MgO," *Applied Physics Letters,* vol. 125, no. 4, 2024, doi: 10.1063/5.0207170.

[83] Y. Miura, S. Muramoto, K. Abe, and M. Shirai, "First-principles study of tunneling magnetoresistance in Fe/MgAl${}_{2}$O${}_{4}$/Fe(001) magnetic tunnel junctions," *Physical Review B,* vol. 86, no. 2, p. 024426, 07/20/ 2012, doi: 10.1103/PhysRevB.86.024426.

[84] Z. H. Yuan, L. Huang, J. F. Feng, Z. C. Wen, D. L. Li, X. F. Han, T. Nakano, T. Yu, and H. Naganuma, "Double-pinned magnetic tunnel junction sensors with spin-valve-like sensing layers," *Journal of Applied Physics,* vol. 118, no. 5, 2015, doi: 10.1063/1.4927840.

[85] K. Ono, T. Daibou, S.-J. Ahn, Y. Sakuraba, T. Miyakoshi, T. Morita, Y. Kikuchi, M. Oogane, Y. Ando, and T. Miyazaki, "Tunneling spectroscopy in CoFeB/MgO/CoFeB magnetic tunnel junctions," *Journal of Applied Physics,* vol. 99, no. 8, 2006, doi: 10.1063/1.2173628.

[86] M. Covington, J. Nowak, and D. Song, "Magnetic tunnel junction performance versus barrier thickness: NiFe/AlOx/NiFe junctions fabricated from a wedged Al layer," *Applied Physics Letters,* vol. 76, no. 26, pp. 3965-3967, 2000, doi: 10.1063/1.126836.

[87] K. Xu, T. Wang, Y. Liu, J. Yu, Z. Li, J. Meng, H. Zhu, Q. Sun, D. W. Zhang, and L. Chen, "Improved Ferroelectricity and Tunneling Electroresistance by Inducing the ZrO2 Intercalation Layer in La:HfO2 Thin Films," *ACS Applied Electronic Materials,* vol. 6, no. 2, pp. 1055-1062, 2024/02/27 2024, doi: 10.1021/acsaelm.3c01496.

[88] Y. Zhang, X. H. Yan, Y. D. Guo, and Y. Xiao, "Negative tunneling magnetoresistance of Fe/MgO/NiO/Fe magnetic tunnel junction: Role of spin mixing and interface state," *Applied Physics Letters,* vol. 111, no. 7, 2017, doi: 10.1063/1.4999764.

[89] T. Newhouse-Illige, Y. H. Xu, Y. H. Liu, S. Huang, H. Kato, C. Bi, M. Xu, B. J. LeRoy, and W. G. Wang, "Temperature dependence of interlayer coupling in perpendicular magnetic tunnel junctions with GdOX barriers," *Applied Physics Letters,* vol. 112, no. 7, 2018, doi: 10.1063/1.5002586.

[90] N. Ghobadi, R. Daqiq, and S. M. Mirebrahimi, "Band-pass magnetic tunnel junctions with β-Ga2O3 semiconductors for spin-filtering goals," *Micro and Nanostructures,* vol. 169, p. 207359, 2022/09/01/ 2022, doi: https://doi.org/10.1016/j.micrna.2022.207359.

[91] M. Oogane, K. Fujiwara, A. Kanno, T. Nakano, H. Wagatsuma, T. Arimoto, S. Mizukami, S. Kumagai, H. Matsuzaki, N. Nakasato, and Y. Ando, "Sub-pT magnetic field detection by tunnel magneto-resistive sensors," *Applied Physics Express,* vol. 14, no. 12, p. 123002, 2021/11/22 2021, doi: 10.35848/1882-0786/ac3809.

[92] T. Nakano, K. Fujiwara, and M. Oogane, "Tunnel-magnetoresistance sensors with sub-pT detectivity for detecting bio-magnetic fields," *Applied Physics Letters,* vol. 126, no. 16, 2025, doi: 10.1063/5.0263879.

[93] T. Nakano, K. Fujiwara, M. Tsunoda, S. Kumagai, and M. Oogane, "Enhanced sensitivity and thermal tolerance in tunnel magnetoresistance sensor using Ta-doped CoFeSiB soft magnetic layer," *Applied Physics Letters,* vol. 123, no. 7, 2023, doi: 10.1063/5.0162276.

[94] J. Vyhnánek, M. Janošek, and P. Ripka, "AMR gradiometer for mine detection," *Sensors and Actuators A: Physical,* vol. 186, pp. 100-104, 2012/10/01/ 2012, doi: https://doi.org/10.1016/j.sna.2012.03.007.

[95] B. D. Kilgore, "A Wideband Magnetoresistive Sensor for Monitoring Dynamic Fault Slip in Laboratory Fault Friction Experiments," *Sensors,* vol. 17, no. 12, p. 2790, 2017. [Online]. Available: https://www.mdpi.com/1424-8220/17/12/2790.

[96] A. L. Herrera-May, J. C. Soler-Balcazar, H. Vázquez-Leal, J. Martínez-Castillo, M. O. Vigueras-Zuñiga, and L. A. Aguilera-Cortés, "Recent Advances of MEMS Resonators for Lorentz Force Based Magnetic Field Sensors: Design, Applications and Challenges," *Sensors,* vol. 16, no. 9, p. 1359, 2016. [Online]. Available: https://www.mdpi.com/1424-8220/16/9/1359.

[97] A. L. Herrera-May, L. A. Aguilera-Cortés, P. J. García-Ramírez, and E. Manjarrez, "Resonant Magnetic Field Sensors Based On MEMS Technology," *Sensors,* vol. 9, no. 10, pp. 7785-7813, 2009. [Online]. Available: https://www.mdpi.com/1424-8220/9/10/7785.

[98] Z. Zhao, M. Toda, and T. Ono, "A resonant magnetic microsensor based on magnetic torque with piezoresistive readout," *Applied Physics Letters,* vol. 124, no. 25, 2024, doi: 10.1063/5.0207431.

[99] A. L. Herrera-May, P. J. García-Ramírez, L. A. Aguilera-Cortés, J. Martínez-Castillo, A. Sauceda-Carvajal, L. García-González, and E. Figueras-Costa, "A resonant magnetic field microsensor with high quality factor at atmospheric pressure," *Journal of Micromechanics and Microengineering,* vol. 19, no. 1, p. 015016, 2008/11/28 2009, doi: 10.1088/0960-1317/19/1/015016.

[100] Z. Kádár, A. Bossche, P. M. Sarro, and J. R. Mollinger, "Magnetic-field measurements using an integrated resonant magnetic-field sensor," *Sensors and Actuators A: Physical,* vol. 70, no. 3, pp. 225-232, 1998/10/30/ 1998, doi: https://doi.org/10.1016/S0924-4247(98)00143-5.

[101] C. Tu, X.-h. Ou-Yang, Y.-j. Wu, and X.-s. Zhang, "Single-structure 3-axis Lorentz force magnetometer based on an AlN-on-Si MEMS resonator," *Microsystems & Nanoengineering,* vol. 10, no. 1, p. 58, 2024/05/09 2024, doi: 10.1038/s41378-024-00696-3.

[102] S. B. Mbarek, N. Alcheikh, H. M. Ouakad, and M. I. Younis, "Highly sensitive low field Lorentz-force MEMS magnetometer," *Scientific Reports,* vol. 11, no. 1, p. 21634, 2021/11/04 2021, doi: 10.1038/s41598-021-01171-z.

[103] J. J. Valle, J. M. Sánchez-Chiva, D. Fernández, and J. Madrenas, "Design, fabrication, characterization and reliability study of CMOS-MEMS Lorentz-force magnetometers," *Microsystems & Nanoengineering,* vol. 8, no. 1, p. 103, 2022/09/16 2022, doi: 10.1038/s41378-022-00423-w.

[104] H. Savage, A. Clark, and J. Powers, "Magnetomechanical coupling and ΔE effect in highly

magnetostrictive rare earth - Fe2compounds," *IEEE Transactions on Magnetics,* vol. 11, no. 5, pp. 1355-1357, 1975, doi: 10.1109/TMAG.1975.1058791.

[105] G. Chen, S. Koizumi, Y. Koide, and M. Liao, "Low-Energy Dissipation Diamond MEMS," *Accounts of Materials Research,* vol. 5, no. 9, pp. 1087-1096, 2024/09/27 2024, doi: 10.1021/accountsmr.4c00139.

[106] M. Liao, "Progress in semiconductor diamond photodetectors and MEMS sensors," *Functional Diamond,* vol. 1, no. 1, pp. 29-46, 2022/01/14 2022, doi: 10.1080/26941112.2021.1877019.

[107] O. Auciello and D. M. Aslam, "Review on advances in microcrystalline, nanocrystalline and ultrananocrystalline diamond films-based micro/nano-electromechanical systems technologies," *Journal of Materials Science,* vol. 56, no. 12, pp. 7171-7230, 2021/04/01 2021, doi: 10.1007/s10853-020-05699-9.

[108] M. Liao, S. Hishita, E. Watanabe, S. Koizumi, and Y. Koide, "Suspended Single-Crystal Diamond Nanowires for High-Performance Nanoelectromechanical Switches," *Advanced Materials,* vol. 22, no. 47, pp. 5393-5397, 2010, doi: https://doi.org/10.1002/adma.201003074.

[109] Z. Zhang, L. Sang, J. Huang, L. Wang, S. Koizumi, and M. Liao, "Tailoring the magnetic properties of galfenol film grown on single-crystal diamond," *Journal of Alloys and Compounds,* vol. 858, p. 157683, 2021/03/25/ 2021, doi: https://doi.org/10.1016/j.jallcom.2020.157683.

[110] Z. Zhang, H. Wu, L. Sang, Y. Takahashi, J. Huang, L. Wang, M. Toda, I. M. Akita, Y. Koide, S. Koizumi, and M. Liao, "Enhancing Delta E Effect at High Temperatures of Galfenol/Ti/Single-Crystal Diamond Resonators for Magnetic Sensing," *ACS Applied Materials & Interfaces,* vol. 12, no. 20, pp. 23155-23164, 2020/05/20 2020, doi: 10.1021/acsami.0c06593.

[111] Z. Zhang, W. Zhao, G. Chen, M. Toda, S. Koizumi, Y. Koide, and M. Liao, "On-chip Diamond MEMS Magnetic Sensing through Multifunctionalized Magnetostrictive Thin Film," *Advanced Functional Materials,* vol. 33, no. 27, p. 2300805, 2023, doi: https://doi.org/10.1002/adfm.202300805.

[112] Z. Zhang, K. Gu, G. Chen, L. Sang, T. Teraji, Y. Koide, S. Koizumi, M. Toda, and M. Liao, "Highly Reliable Diamond MEMS Dual Sensor for Magnetic Fields and Temperatures with Self-Recognition Algorithms," *Advanced Materials Technologies,* vol. 9, no. 13, p. 2400153, 2024, doi: https://doi.org/10.1002/admt.202400153.

[113] Y. Wang, D. Gray, D. Berry, J. Gao, M. Li, J. Li, and D. Viehland, "An Extremely Low Equivalent Magnetic Noise Magnetoelectric Sensor," *Advanced Materials,* vol. 23, no. 35, pp. 4111-4114, 2011, doi: https://doi.org/10.1002/adma.201100773.

[114] M. Bichurin, R. Petrov, O. Sokolov, V. Leontiev, V. Kuts, D. Kiselev, and Y. Wang, "Magnetoelectric Magnetic Field Sensors: A Review," *Sensors,* vol. 21, no. 18, p. 6232, 2021. [Online]. Available: https://www.mdpi.com/1424-8220/21/18/6232.

[115] G. Yuan, R. Xu, H. Wu, Y. Xing, C. Yang, R. Zhang, W. Tang, Y. Wang, and Y. Wang, "High-

temperature multiferroic magnetoelectric sensors," *Applied Physics Letters,* vol. 121, no. 19, 2022, doi: 10.1063/5.0124352.

[116] M. Liao, Y. Gotoh, H. Tsuji, K. Nakajima, M. Imura, and Y. Koide, "Piezoelectric Pb(Zr0.52Ti0.48)O3 thin films on single crystal diamond: Structural, electrical, dielectric, and field-effect-transistor properties," *Journal of Applied Physics,* vol. 107, no. 2, 2010, doi: 10.1063/1.3282706.

[117] M. Liao, K. Nakajima, M. Imura, and Y. Koide, "Improved ferroelectric properties of Pb(Zr0.52,Ti0.48)O3 thin film on single crystal diamond using CaF2 layer," *Applied Physics Letters,* vol. 96, no. 1, 2010, doi: 10.1063/1.3291056.

[118] H. Wu, L. Sang, Y. Li, T. Teraji, T. Li, M. Imura, J. You, Y. Koide, M. Toda, and M. Liao, "Reducing intrinsic energy dissipation in diamond-on-diamond mechanical resonators toward one million quality factor," *Physical Review Materials,* vol. 2, no. 9, p. 090601, 09/28/ 2018, doi: 10.1103/PhysRevMaterials.2.090601.

[119] M. A. Vallée and S. Mazur, "Advances in Magnetic and Electromagnetic Techniques for Mineral Exploration: Enhancing Resource Discovery," *Minerals,* vol. 15, no. 6, p. 595, 2025. [Online]. Available: https://www.mdpi.com/2075-163X/15/6/595.

[120] D. Vihywuseh, C. T. Tabod, E. N. Ndikum, A. R. Khan, and D. A. Fuen, "Unveiling the subsurface geological structure of the centre region, cameroon, with aeromagnetic data analysis," (in eng), *Sci Rep,* vol. 15, no. 1, p. 33296, Sep 26 2025, doi: 10.1038/s41598-025-08077-0.

[121] P. A. Polito, B. T. Karykowski, F. C. Best, and A. J. Crawford, "Magnetite-hosted Cu-PGE and Fe-sulfide mineralization in 1078 Ma layered mafic intrusions in the west Musgraves region of Western Australia," *Ore Geology Reviews,* vol. 90, pp. 510-531, 2017/11/01/ 2017, doi: https://doi.org/10.1016/j.oregeorev.2017.05.003.

[122] M. Zientek, "Magmatic ore deposits in layered intrusions - Descriptive model for reef-type PGE and contact-type Cu-Ni-PGE deposits," in "Open-File Report," Reston, VA, Report 2012-1010, 2012. [Online]. Available: https://pubs.usgs.gov/publication/ofr20121010

[123] S. An, C. Yao, Z. Zhang, J. Wang, W. Wang, Q. Qiao, and S. Wang, "Structural analysis of magmatic Ni-Cu sulfide deposit based on high-precision magnetic surveying: A case study of the Baixintan Ni-Cu deposit in eastern Tianshan, NW China," *Ore Geology Reviews,* vol. 186, p. 106916, 2025/11/01/ 2025, doi: https://doi.org/10.1016/j.oregeorev.2025.106916.

[124] P. J. Williams, M. D. Barton, D. A. Johnson, L. Fontboté, A. d. Haller, G. Mark, N. H. S. Oliver, and R. Marschik, "Iron Oxide Copper-Gold Deposits: Geology, Space-Time Distribution, and Possible Modes of Origin," in *One Hundredth Anniversary Volume*, J. W. Hedenquist, J. F. H. Thompson, R. J. Goldfarb, and J. P. Richards Eds.: Society of Economic Geologists, 2005, p. 0.

[125] L. Milani, L. Oosthuizen, T. M. Owen-Smith, G. M. Bybee, B. Hayes, J. Lehmann, and H. A. Jelsma, "Magnetite geochemistry as a proxy for metallogenic processes: A study on sulfide-

mineralized mafic–ultramafic intrusions peripheral to the Kunene Complex in Angola and Namibia," *Mineralium Deposita,* vol. 60, no. 2, pp. 551-580, 2025/03/01 2025, doi: 10.1007/s00126-024-01288-x.

[126] O. K. Likkason, "Exploring and Using the Magnetic Methods," in *Advanced Geoscience Remote Sensing*, M. Marghany Ed. London: IntechOpen, 2014.

[127] "Magnetic surveying," in *Environmental and Engineering Geophysics*, P. V. Sharma Ed. Cambridge: Cambridge University Press, 1997, pp. 65-111.

[128] I. Ugarte-Goicuría, D. Guerrero-Sevilla, P. Carrasco-Garcia, J. Carrasco-Garcia, and D. González-Aguilera, "Aerial Drone Magnetometry for the Detection of Subsurface Unexploded Ordnance (UXO) in the San Gregorio Experimental Site (Zaragoza, Spain)," in *Preprints*, ed: Preprints, 2025.

[129] Q. Zhang, K. Zhou, M. Deng, Q. Zhang, Y. Feng, and L. Liu, "Development of a High-Precision Deep-Sea Magnetic Survey System for Human-Occupied Vehicles," *Electronics,* vol. 13, no. 18, p. 3611, 2024. [Online]. Available: https://www.mdpi.com/2079-9292/13/18/3611.

[130] J. Yan, Z. Wang, J. Wang, and J. Song, "Using marine magnetic survey data to identify a gold ore-controlling fault: a case study in Sanshandao fault, eastern China," *Journal of Geophysics and Engineering,* vol. 15, no. 3, pp. 729-738, 2018, doi: 10.1088/1742-2140/aa9c69.

[131] L. Tang, Y. Zhang, G. Zhou, W. Zhao, Q. Bian, Z. Li, S. Liu, and J. Gao, "Calibration of magnetic interfering coefficients for shipboard three-component magnetometers using a geomagnetic field simulator," *Measurement,* vol. 257, p. 118968, 2026/01/15/ 2026, doi: https://doi.org/10.1016/j.measurement.2025.118968.

[132] T. A. Adagunodo, L. A. Sunmonu, and A. A. Adeniji, "AN OVERVIEW OF MAGNETIC METHOD IN MINERAL EXPLORATION," *Journal of Global Ecology and Environment,* vol. 3, no. 1, pp. 13-28, 07/23 2015. [Online]. Available: https://ikprress.org/index.php/JOGEE/article/view/321.

[133] G. Yu, X. Hu, J. Fang, Y. Yang, Y. Zhang, J. Lin, J. Liu, and L. Qian, "Application of Multiple Geophysical Exploration Methods in the Exploration of Marine Sand Resources in the Northern Offshore Waters of the South China Sea," *Journal of Marine Science and Engineering,* vol. 12, no. 9, p. 1561, 2024. [Online]. Available: https://www.mdpi.com/2077-1312/12/9/1561.

[134] R. Y. Choi, A. S. Coyner, J. Kalpathy-Cramer, M. F. Chiang, and J. P. Campbell, "Introduction to Machine Learning, Neural Networks, and Deep Learning," (in eng), *Transl Vis Sci Technol,* vol. 9, no. 2, p. 14, Feb 27 2020, doi: 10.1167/tvst.9.2.14.

[135] R. Zuo and E. J. M. Carranza, "Support vector machine: A tool for mapping mineral prospectivity," *Computers & Geosciences,* vol. 37, no. 12, pp. 1967-1975, 2011/12/01/ 2011, doi: https://doi.org/10.1016/j.cageo.2010.09.014.

[136] P. Josso, A. Hall, C. Williams, T. Le Bas, P. Lusty, and B. Murton, "Application of random-forest machine learning algorithm for mineral predictive mapping of Fe-Mn crusts in the World Ocean,"

Ore Geology Reviews, vol. 162, p. 105671, 2023/11/01/ 2023, doi: https://doi.org/10.1016/j.oregeorev.2023.105671.

[137] Y. Mu, X. Zhang, W. Xie, and Y. Zheng, "Automatic Detection of Near-Surface Targets for Unmanned Aerial Vehicle (UAV) Magnetic Survey," *Remote Sensing,* vol. 12, no. 3, p. 452, 2020. [Online]. Available: https://www.mdpi.com/2072-4292/12/3/452.

[138] S. Wu, S. Thoram, J. Sun, W. W. Sager, and J. Chen, "Characterizing Marine Magnetic Anomalies: A Machine Learning Approach to Advancing the Understanding of Oceanic Crust Formation," *Journal of Geophysical Research: Solid Earth,* vol. 130, no. 2, p. e2024JB030682, 2025, doi: https://doi.org/10.1029/2024JB030682.

[139] F. E. Yigzew, H. Kim, D. A. Beyene, G. K. Likasa, and S. Park, "Machine learning-augmented magneto-hall sensor network analysis for optimized MFL imaging and detection in ferromagnetic structural component," *Sensors and Actuators A: Physical,* vol. 397, p. 117277, 2026/01/01/ 2026, doi: https://doi.org/10.1016/j.sna.2025.117277.

[140] T. Siddique and M. S. Mahmud, "Physics-Enhanced TinyML for Real- Time Detection of Ground Magnetic Anomalies," *IEEE Access,* vol. 12, pp. 25372-25384, 2024, doi: 10.1109/ACCESS.2024.3362346.

[141] S. M. Graham, A. J. Newman, C. J. Stephen, A. M. Edmonds, D. J. Twitchen, M. L. Markham, and G. W. Morley, "On the road with a diamond magnetometer," *Diamond and Related Materials,* vol. 152, p. 111945, 2025/02/01/ 2025, doi: https://doi.org/10.1016/j.diamond.2025.111945.

[142] M. Cambria, S. Chand, C. M. Reiter, and S. Kolkowitz, "Scalable Parallel Measurement of Individual Nitrogen-Vacancy Centers," *Physical Review X,* vol. 15, no. 3, p. 031015, 07/14/ 2025, doi: 10.1103/jdzq-jbfz.

[143] M. Djamal and R. Ramli, "Giant Magnetoresistance Sensors Based on Ferrite Material and Its Applications," in *Magnetic Sensors - Development Trends and Applications*, A. Asfour Ed. London: IntechOpen, 2017.

[144] M. Díaz-Michelena, "Small Magnetic Sensors for Space Applications," *Sensors,* vol. 9, no. 4, pp. 2271-2288, 2009. [Online]. Available: https://www.mdpi.com/1424-8220/9/4/2271.